Cell Metabolism
Short Article

# Adaptive Downregulation of Mitochondrial Function in Down Syndrome

Pablo Helguera,[1,6] Jaqueline Seiglie,[1] Jose Rodriguez,[4] Michael Hanna,[1] Gustavo Helguera,[5] and Jorge Busciglio[1,2,3,*]
[1]Department of Neurobiology and Behavior
[2]Institute for Memory Impairments and Neurological Disorders
[3]Center for the Neurobiology of Learning and Memory
University of California, Irvine, Irvine, CA 92697, USA
[4]Molecular Biology Institute, University of California, Los Angeles, Los Angeles, CA 90095, USA
[5]Cátedra de Tecnología Farmacéutica I, Facultad de Farmacia y Bioquímica, Universidad de Buenos Aires, Junín 954 6° Piso, Ciudad Autónoma de Buenos Aires C1113AAD, Argentina
[6]Laboratorio de Neuropatologia Experimental, Instituto de Investigación Médica Mercedes y Martín Ferreyra, INIMEC-CONICET, Universidad Nacional de Córdoba, Friuli 2434, Córdoba 5016, Argentina
*Correspondence: jbuscigl@uci.edu
http://dx.doi.org/10.1016/j.cmet.2012.12.005

## SUMMARY

**Mitochondrial dysfunction and oxidative stress are common features of Down syndrome (DS). However, the underlying mechanisms are not known. We investigated the relationship between abnormal energy metabolism and oxidative stress with transcriptional and functional changes in DS cells. Impaired mitochondrial activity correlated with altered mitochondrial morphology. Increasing fusion capacity prevented morphological but not functional alterations in DS mitochondria. Sustained stimulation restored mitochondrial functional parameters but increased reactive oxygen species production and cell damage, suggesting that reduced DS mitochondrial activity is an adaptive response for avoiding injury and preserving basic cellular functions. Network analysis of genes overexpressed in DS cells demonstrated functional integration in pathways involved in energy metabolism and oxidative stress. Thus, although preventing extensive oxidative damage, mitochondrial downregulation may contribute to increased susceptibility of individuals with DS to clinical conditions in which altered energy metabolism may play a role, such as Alzheimer's disease, diabetes, and some types of autistic spectrum disorders.**

## INTRODUCTION

Down Syndrome (DS), or trisomy 21, is characterized by a complex phenotype that includes both developmental and chronic health complications (Roizen and Patterson, 2003). Altered mitochondrial activity and oxidative stress have long been associated with DS (Arbuzova et al., 2002; Brooksbank and Balazs, 1984). For example, DS cortical neurons exhibit higher production of intracellular reactive oxygen species (ROS) and lipid peroxidation, which compromise neuronal survival (Busciglio and Yankner, 1995), and both DS neurons and astrocytes display an abnormal pattern of protein processing consistent with chronic energy deficits (Busciglio et al., 2002). Altered mitochondrial activity has been reported in DS fibroblasts (Valenti et al., 2011), and mitochondrial DNA mutations were found in DS brain tissue (Coskun and Busciglio, 2012).

Microarray profiling of DS neural progenitor cells indicates an association between altered chromosome 21 gene expression and cellular injury mediated by oxidative stress (Esposito et al., 2008). Similarly, DS amniotic fluid samples show altered activity of oxidative-stress-associated genes early in pregnancy (Slonim et al., 2009).

Oxidative stress has widely been associated with impaired mitochondrial function and morphology, leading to the disruption of cable-like morphology and impaired ATP production (Knott et al., 2008). Functional elongated mitochondria undergo remodeling in response to energy requirements, cellular stress or calcium oscillations (Chan, 2006), and mitochondrial fragmentation is correlated with reduced ATP and increased ROS production (Yu et al., 2006). With these considerations in mind, we assessed the relationship between mitochondrial dysfunction, altered mitochondrial morphology, oxidative stress, and transcriptional changes in DS cells. The results indicate that reduced mitochondrial metabolism in DS is associated with an adaptive response for preventing oxidative damage and preserving cellular function.

## RESULTS

### Altered Morphology and Increased Oxidative Stress in DS Mitochondria

There is a close relationship between mitochondrial morphology and functional state. Marked alterations in mitochondrial function previously identified in DS cells (Busciglio et al., 2002) led us to examine mitochondrial morphology in normal (NL) and DS astrocytes (Figure 1A). Mitochondria were classified according to size in three groups: $\leq 3$ μm, 3.1–15 μm, and $\geq 15.1$ μm. The mitochondrial network in DS cells is more fragmented, as demonstrated by a significant increase in the number of shorter

mitochondria (both ≤3 μm and 3.1–15 μm groups) and a reduced number of longer mitochondria (≥15.1 μm) (Figure 1B). Electron transport chain protein expression was similar in NL and DS cells (Figure S1A available online), indicating that morphological and functional changes were not related to changes in DS mitochondrial mass. We found shorter mitochondria in other DS primary cell types, including fibroblasts (Figure S1B), neurons, and pancreatic cells (see below), suggesting generalized perturbations in DS mitochondrial function and morphology. Altered mitochondrial morphology is associated with functional impairment in DS cells, which exhibit reduced mitochondrial membrane potential (MMP), oxidoreductase (ox/red) activity, and ATP generation (Busciglio et al., 2002). Given the close association between mitochondrial morphology and function, we investigated whether functional changes could be reverted by manipulating DS mitochondrial morphology. Mitofusin 1 (mfn1), a critical regulator of mitochondrial fusion, enhanced DS mitochondrial fusion (Figure 1C), increased the number of tubular mitochondria, and reduced the number of puncta-like ones (Figure 1D). However, mfn1 expression had no effect on MMP (Figures 1E and 1F). Similar results were obtained with mfn2 (data not shown).

Because correcting morphological alterations did not enhance DS mitochondrial function, we investigated whether DS cells actually possess the capacity to increase mitochondrial activity after metabolic stimulation. To achieve a sustained stimulation of mitochondria, we used 5 mM creatine for 7 days (Andres et al., 2005). ATP level, ox/red activity, and MMP were reduced in DS cells (Figures 1G–1I). Creatine did not affect mitochondrial activity in NL cells, but it markedly increased ox/red activity, ATP levels, and MMP in DS cells (Figures 1G–1I), indicating that upon stimulation, DS mitochondria possess the capacity to increase energy metabolism. However, creatine reduced DS cell survival, whereas it had no effect on the viability of NL cultures (Figure 1J). One potential consequence of enhanced mitochondrial activity is increased free-radical generation, which has been previously reported in DS (Busciglio and Yankner, 1995). Under basal conditions, DS cells exhibited 3-fold higher levels of superoxide, expressed as the ratio of MitoSOX Red over MitoTracker Green fluorescence area (NL: 4 ± 1%, DS: 16 ± 3%)(Figures 1K and 1L). Creatine nearly doubled superoxide levels in both NL and DS mitochondria (NL: 12 ± 5%, DS: 31 ± 9%) (Figure 1L). In addition, creatine increased lipid peroxidation in DS cells (Figure 1M), consistent with the observed decrease in cell viability (Figure 1J). Thus, DS mitochondria are capable of sustaining increased activity. However, this resulted in increased ROS generation, cellular damage, and cell death.

## Gene Expression in DS Cells Is Associated with a Pattern of Chronic Oxidative Stress

We performed a broad-spectrum microarray analysis using messenger RNA (mRNA) from three NL and five DS astrocyte cultures. The microarray output was validated for several genes (Figure S2A and Supplemental Experimental Procedures). A total of 92 genes discriminated between NL and DS samples (Figure 2A). Sixty genes were upregulated (>1.45-fold), 11 of which are located in chromosome 21 (highlighted in red, Figure 2A). The other 32 genes were downregulated (<0.65-fold), none of which are localized in chromosome 21. Although chromosome 21 genes were overrepresented among upregulated genes (18.3%), the majority of them (81.7%) were located in other chromosomes.

Ingenuity analysis generated a network illustrating the relationship between overexpressed genes (Figure S2B). Three main pathways related to the upregulated genes were identified: (1) Nfr2-associated oxidative stress response, (2) oxidative stress, and (3) mitochondrial dysfunction (Figure S2B). All three pathways support the presence of chronic oxidative stress in DS. To explore the relationship between gene expression and oxidative stress, we evaluated the expression of "DS signature genes" in NL astrocytes subjected to mild oxidative stress (50 μM $H_2O_2$ for 12 hr). In general, the changes in DS signature genes in NL astrocytes plus $H_2O_2$ were smaller in magnitude than the ones in DS cells. However, in most cases, the expression in NL astrocytes plus $H_2O_2$ shifted in the same direction as in DS cells, placing their profile somewhere between the DS and NL profiles (Figure 2B) and further suggesting that oxidative stress drives gene expression changes in DS cells.

## Altered Mitochondrial Morphology and Function in DS Neurons

Given that cells with high energy demands are especially susceptible to mitochondrial alterations, we assessed mitochondrial function in DS neurons. Mitochondria were classified according to size as: puncta-like mitochondria (≤300 nm in diameter) (Figure 3A, small arrow); globular mitochondria (600–1200 nm in diameter) (Figure 3A, arrowhead); and tubular mitochondria (≥500 nm) (Figure 3A, big arrow). Mitochondria were also shorter in DS neurons (Figure 3B). Similar results were obtained by using MitoTracker Green and JC-1 (Figures S3A and S3B). JC-1 labeling revealed a marked reduction in MMP, which was accompanied by a decrease in ox/red activity and ATP levels (Figure 3C and Figures S3D and S3E). JC-1 formed aggregates in discrete domains of tubular and puncta-like mitochondria, but never in globular mitochondria (Figure S3B), which frequently colocalized with lisosomal markers (Figure S3C), suggesting that the latter represent a subset of inactive or damaged mitochondria. Interestingly, discrete energized regions in both NL and DS mitochondria (Figures S3B and S3D) point to the existence of specific domains with different activities within individual mitochondria in human neurons.

## Impaired Mitochondrial Transport in DS Neurons

Because axonal transport is highly dependent on ATP and is critical for synaptic activity and neuronal survival (Brady, 1991), we assessed anterograde mitochondrial transport in DS neurons. DS mitochondria moved slower (350 ± 60 nm/s) than NL mitochondria (1,100 ± 130 nm/s, Figures 3D and 3E). Conversely, we observed a higher number of moving mitochondria at any given time point in DS cells (38 ± 7% in DS cells; 20 ± 3% in NL cells; Figure 3F), which may be a compensatory change. Both parameters were affected by creatine, which also increased the number of energized mitochondria in DS neurons (Figure S3E). Thus, reduced mitochondrial function and ATP levels lead to impaired mitochondrial transport in DS neurons.

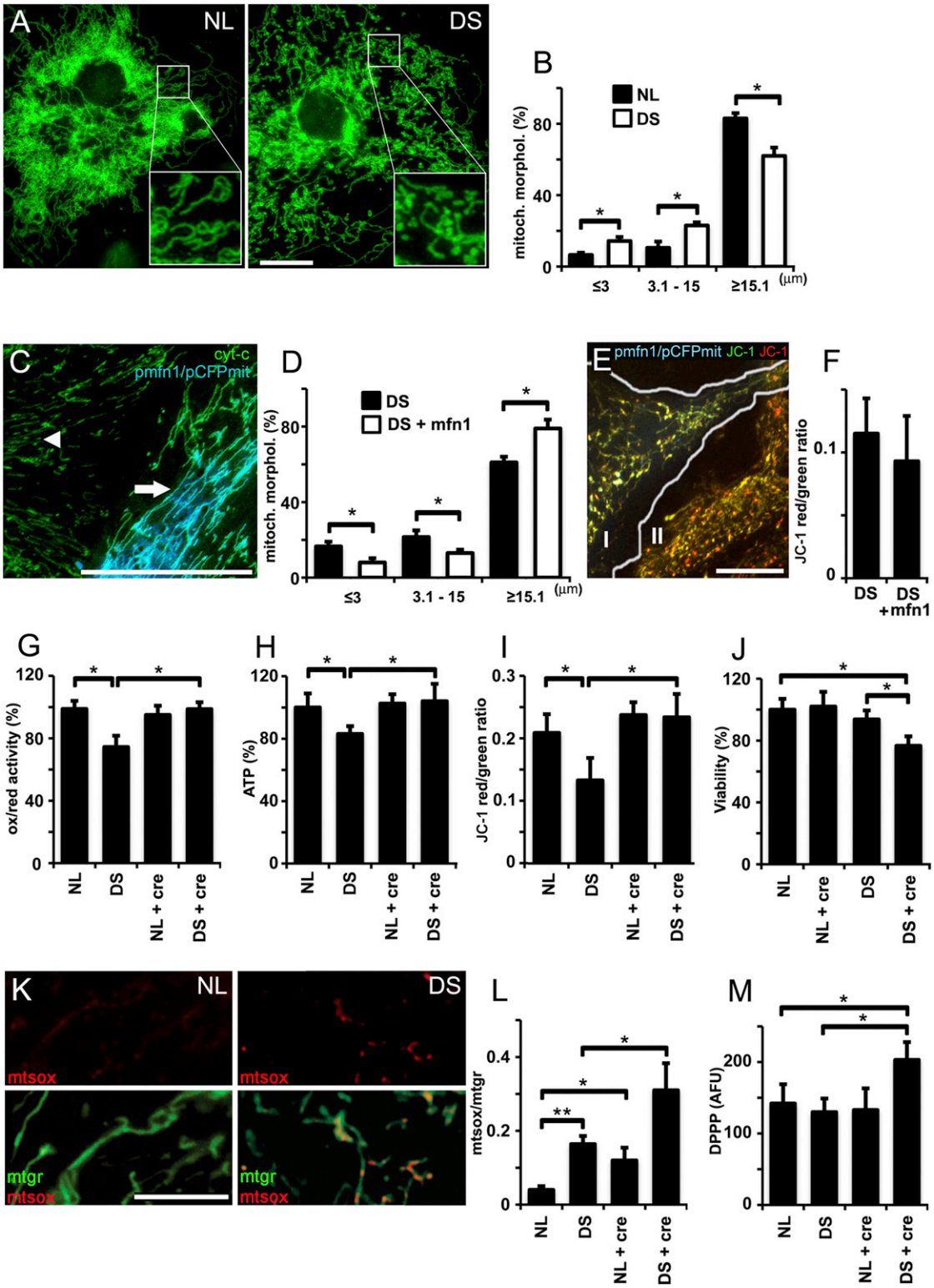


**Figure 1. Mitochondrial Alterations in DS Astrocytes**

(A) NL and DS astrocytes were stained with MitoTracker Green. Elongated mitochondria predominate in NL astrocytes (NL, inset), whereas the number of puncta-like and globular mitochondria was higher in DS astrocytes (DS, inset). The scale bar represents 10 μm.

(B) Quantification of mitochondrial shapes binned according to length and size in NL and DS astrocytes. *$p < 0.05$.

(C) A DS astrocyte (arrow) coexpressing pmfn1 and pCFPmit shows tubular mitochondria. In an adjacent, nontransfected DS cell (arrowhead), cytochrome C immunofluorescence (IF) (green) illustrates shorter mitochondrial shapes. The scale bar represents 20 μm.

*(legend continued on next page)*

### Functional Alterations in DS Pancreatic β Cells Are Associated with Reduced Energy Metabolism

Pancreatic cells also require relatively high metabolic rates to maintain secretory function. We examined mitochondrial morphology, activity, and basal insulin secretion in NL and DS islet cell clusters (ICCs) (Figure 4A). Both fetal pancreas and ICCs expressed insulin and glucagon (Figure 4B, subpanels I and II). Mitochondria in β cells were visualized with anti-cytochrome C (Figure 4C). DS β cells exhibited fragmented mitochondria (DS, Figure 4D), as did NL β cells treated with 5 μM FCCP for 1 hr (NL+FCCP, Figure 4D). Ox/red activity was reduced in DS ICCs (73% ± 9% of NL ICC activity normalized as 100%). Given that mitochondrial dysfunction is associated with intracellular amyloid β accumulation in DS cells (Busciglio et al., 2002), we assessed whether islet amyloid polypeptide (IAPP, or amylin) accumulates in DS β cells. Insulin and IAPP are coexpressed and localize to the same vesicles in β cells (Figure 4E), which were labeled with A11, a conformation-specific antibody that recognizes IAPP oligomers (Kayed et al., 2007). We found increased A11-positive puncta in DS β cells, 7.3 ± 2.6 puncta per cell in DS cells, and 1.7 ± 1.5 puncta per cell in NL cells; n = 5 in both cases (Figure 4F, arrows). Thus, energy deficits may result in abnormal intracellular accumulation of IAPP in DS β cells.

NL β cells secreted 4-fold more insulin than DS β cells (Figure 4G). In contrast, DS β cells secreted 8-fold more proinsulin than NL β cells (Figure 4H), indicating incomplete processing and reduced insulin secretion. Neither creatine (5 mM) nor antioxidant trolox (50 μM) alone had an effect on insulin or proinsulin secretion. However, when both compounds were added together, we observed a slight increase in insulin (17 ± 5%) and a reduction in proinsulin (24 ± 4%) secretion in DS ICCs (Figures 4G and 4H). None of the treatments had a significant effect on insulin or proinsulin levels in NL cells (data not shown). Thus, mitochondrial downregulation may impair secretory function in DS β cells. The secretory deficits were partially corrected by combined treatment with an energy buffer and an antioxidant, underscoring the link between impaired cellular function, oxidative stress, and mitochondrial alterations in DS.

## DISCUSSION

Chronic oxidative stress and mitochondrial dysfunction are conspicuous features of DS (Arbuzova et al., 2002; Slonim et al., 2009). We found that mitochondrial morphology is consistently altered in DS cells, which exhibit increased fragmentation. Mitofusin overexpression reverted the fragmented phenotype. However, it did not improve MMP in DS cells. Consequently, we investigated whether DS mitochondria actually possessed the capacity to increase ATP production after metabolic stimulation. Creatine increased DS mitochondrial activity and mitochondrial anterograde movement, but it nearly doubled ROS levels, increased lipid peroxidation, and reduced viability in DS cells. Thus, sustained stimulation resulted in increased DS cell damage and death, suggesting that the downregulation of DS mitochondria is part of an adaptive response for avoiding excessive ROS generation and cellular injury.

From a broader perspective, the relationship between mitochondrial morphology and function appears to be context specific, depending on the cell's state and the factors affecting it. For example, in insulinoma cells, ATP-dependent hormone secretion is not affected by mitochondrial fragmentation induced with a dominant negative form of mfn1 but is significantly reduced by hFis1 overexpression, which also generates a fragmented phenotype (Park et al., 2008). In the case of DS primary cells, mitochondria are more fragmented, and both energy production and some cellular functions are impaired. Thus, the balance between mitochondrial morphology and function is complex and is influenced by multiple factors.

We found 92 genes differentially expressed in DS cells. Ingenuity analysis generated a network of overexpressed genes indicative of a transcriptional response to oxidative stress (Figure S2). These changes in gene expression may orchestrate the cellular adaptations required for preserving homeostasis in DS cells, including downregulation of energy metabolism. This possibility is further supported by similar although less pronounced changes in the expression of DS signature genes in NL astrocytes under mild oxidative stress (Figure 2B). Under basal culture conditions, which are nevertheless pro-oxidant, and wherein DS energy metabolism is already impaired (Coskun and Busciglio, 2012; Valenti et al., 2011), the adaptive response would stabilize cell homeostasis at the expense of compromising cellular functions dependent on particular energy requirements, e.g., insulin secretion in β cells or axonal transport in neurons. At the organismal level, this adaptation may contribute to the increased susceptibility of individuals with DS to pathologies in which energy metabolism appears to be compromised,

(D) Morphometric analysis shows a higher frequency of longer mitochondria and a lower frequency of shorter ones in mfn1-expressing DS astrocytes. *p < 0.05.
(E) A DS astrocyte cotransfected with pCFPmit and pmfn1 (subpanel I) shows longer mitochondria (JC-1 green) compared to a nontrasnfected astrocyte (II). The number of energized mitochondria did not change (JC-1 red). The scale bar represents 10 μm.
(F) JC-1 red/green ratio shows no differences in the frequency of energized mitochondria in pmfn1-expressing astrocytes compared to nontransfected cells.
(G–I) Quantification of ATP (G), ox/red activity (H), and MMP (red/green JC-1 fluorescence ratio, I). Treatment with 5 mM creatine (cre) markedly increased all three parameters of mitochondrial activity in DS astrocytes.*p < 0.01.
(J) Quantification of astrocyte viability (LDH). Note the reduction in viability in DS astrocytes treated with creatine (5 mM). *p < 0.05.
(K) NL and DS astrocytes labeled with MitoTracker Green and MitoSOX. Simultaneous staining allows the visualization of superoxide production (mtsox, red) in live-cell mitochondria (mtgr, green). The scale bar represents 20 μm.
(L) Superoxide levels expressed as a MitoSOX/MitoTracker ratio (superoxide signal/total mitochondrial signal). The superoxide level in DS mitochondria was further elevated by treatment with 5 mM creatine (NL + cre, DS + cre). *p < 0.05 and **p < 0.01.
(M) Quantification of lipid peroxidation. DPPP was used for monitoring lipid peroxidation, which is expressed as arbitrary fluorescent units (AFU). DS astrocytes treated with creatine (cre, 5 mM) exhibited a significant increase in lipid peroxidation (139% ± 11.2%). *p < 0.01.
Statistics: (B) and (D), Student's t test; (G)–(J), (L), and (N), two-way ANOVA followed by Tukey's HSD test.
(G–J, L, and M) Values are the mean ± SD; n = 8 independent experiments with cultures derived from different NL and DS brain specimens.

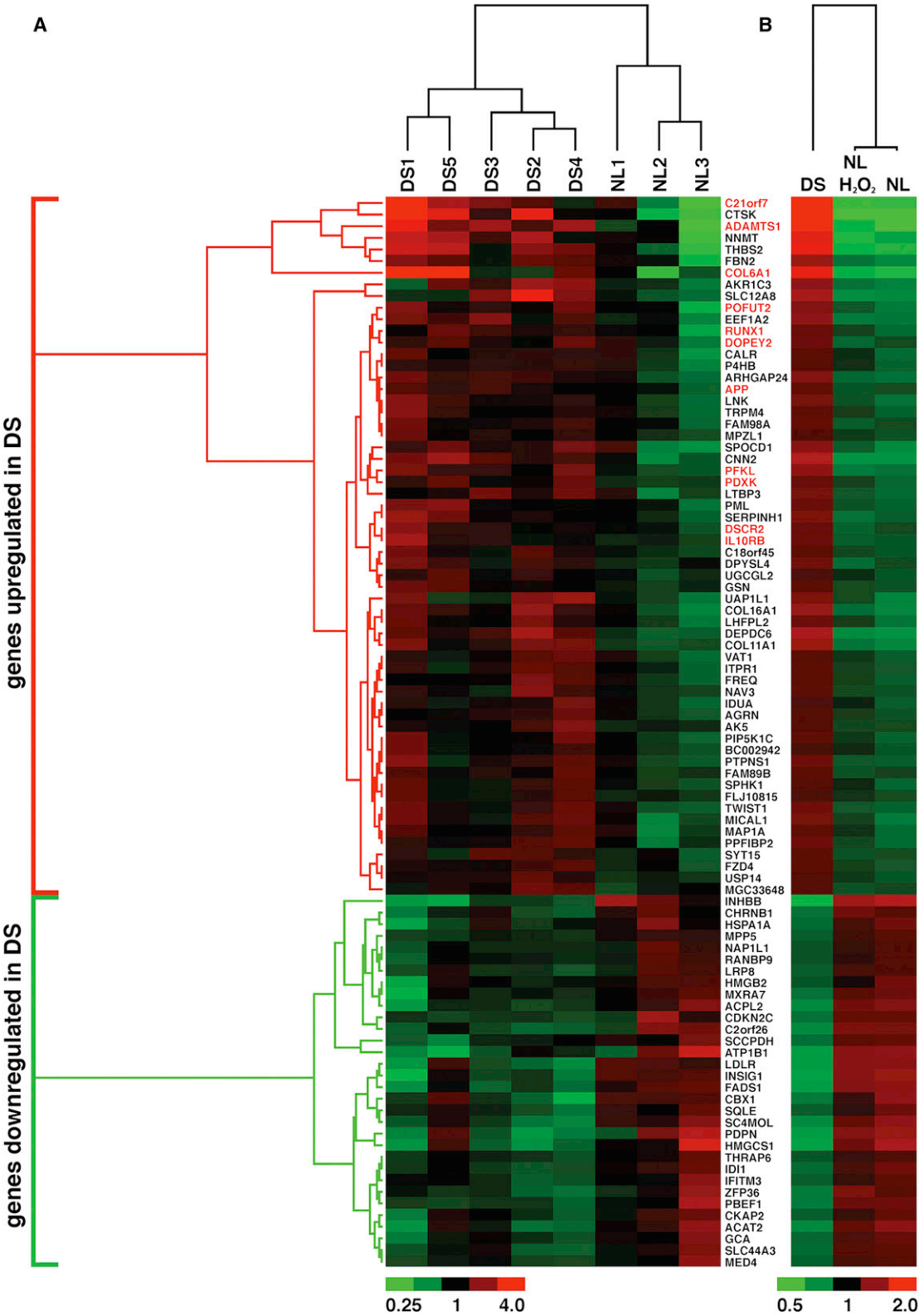


**Figure 2. Gene Expression in DS Cells Is Associated with a Pattern of Chronic Oxidative Stress**

Hierarchical cluster analysis and relative RNA expression in three NL and five DS astrocyte cultures are shown. Expression changes per gene with respect to the average expression across all arrays are shown as a heat map. The fold-change color code is indicated at the bottom. Distance trees represent the relative difference (branching distance) between genes (left) or between conditions (top).

*(legend continued on next page)*

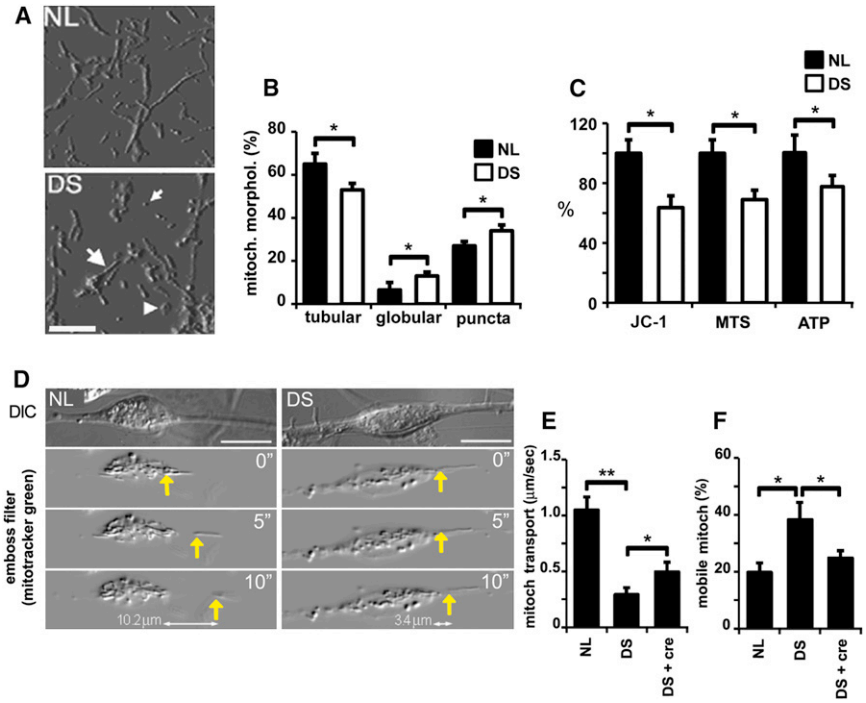


**Figure 3. Altered Mitochondrial Morphology and Function in DS Neurons**

(A) Mitochondria in NL and DS neurons (21 days in vitro) visualized with cytochrome C antibody. Images were processed with an emboss filter. Mitochondria were classified as tubular (large arrow), puncta (small arrow), and globular (arrowhead). The scale bar represents 5 μm.

(B) Quantification of mitochondrial morphotypes expressed as a percentage of the total mitochondrial mass. Tubular mitochondria are reduced whereas puncta- and globular-shaped mitochondria are increased in DS cells. *$p < 0.05$.

(C) Reduced mitochondrial function in DS neurons. MMP is expressed as a JC-1 red/green ratio (JC-1). Ox/red activity (MTS) and ATP levels (ATP) were assessed using commercial assays. The results are expressed as a percentage of the values found in NL cultures. DS cultures exhibit significant reductions in all three parameters. Values for each treatment were normalized to LDH cellular levels. *$p < 0.05$.

(D) Mitochondrial transport in NL and DS neurons (upper panel, differential interference contrast [DIC] images) was recorded after live staining with MitoTracker Green and processed with an emboss filter. Images correspond to 0, 5, and 10 s respectively in both NL and DS neurons (yellow arrows). The traveled distance is specified in the bottom panel. The scale bar represents 10 μm.

(E) Quantification of mitochondrial transport. DS mitochondria move slower than NL mitochondria. Creatine (5 mM; DS+cre) increased DS mitochondrial velocity (cre: 5 mM creatine). *$p < 0.05$ and **$p < 0.01$.

(F) Quantification of mobile mitochondria. NL and DS neurons were labeled with MitoTracker Green. Images acquired at 0 and 20 s time points were subtracted for the generation of a ratio of stationary over moving mitochondria (see Supplemental Experimental Procedures). The number of moving mitochondria was higher in DS neurons, and it was reduced to NL levels by treatment with 5 mM creatine (DS+cre). *$p < 0.01$.

Statistics: (B) and (C), Student's t test; (E) and (F), one-way ANOVA followed by Tukey's HSD test.

such as Alzheimer's disease, diabetes, and some forms of autism (Capone et al., 2005; Esbensen, 2010; Lott and Head, 2005).

Recent studies have underscored the critical role of chronic superoxide production leading to mitochondrial dysfunction, telomere shortening, and replicative senescence in human cells (Passos et al., 2007), further suggesting that the accelerated senescence phenotype characteristic of DS cells (Pallardó et al., 2010) may also be a direct result of cumulative oxidative damage and mitochondrial mutations (Coskun and Busciglio, 2012). Aneuploidies in general are detrimental to organismal and cellular function, altering cell metabolism and decreasing cell proliferation in yeast, mice, and humans, regardless of which chromosome is affected (Williams et al., 2008). In fact, human fibroblasts harboring different aneuploidies display similar increases in sensitivity as well as in common cellular responses to chronic oxidative stress (P.H. and J.B., unpublished data). In this context, DS phenotypes at both the cellular and system levels would arise from the interplay between specific changes in chromosome 21 gene expression, operating on a background of generalized metabolic perturbations and set off by the aneuploid state.

In summary, DS cells exhibit chronic energy deficits that appear to be part of an adaptive response to minimize oxidative damage and preserve cellular homeostasis. Depending on particular energy requirements, specific cellular functions will be affected in different cell types. In the case of DS pancreatic β cells, insulin secretion and proinsulin processing were significantly improved only when antioxidant treatment and mitochondrial stimulation were applied together. Thus, combined therapeutic strategies for preventing free-radical damage and modulating energy metabolism may prove valuable for managing some of the clinical manifestations commonly associated with DS.

## EXPERIMENTAL PROCEDURES

### Cell Cultures

Primary human cortical neuronal and astrocyte cultures were established from ten DS (17–20 weeks of gestational age) and ten age-matched control brain

(A) A total of 92 genes were differentially expressed in DS cells. The DS fingerprint segregated NL from DS samples, each of which was derived from different cultures. A total of 60 genes were upregulated (red bracket), 12 of which are present in chr 21 (highlighted in red). A total of 32 genes were downregulated (green bracket), none of which were located in chr 21.

(B) Relative RNA levels of the 92 genes in (A). The average expression of the three NL and five DS cultures is shown in (A). NL+$H_2O_2$: average expression of the three NL cultures treated with $H_2O_2$ (see Supplemental Experimental Procedures). Note that the expression of DS "signature" genes in $H_2O_2$-treated astrocytes shifts in the same direction as in DS cells.

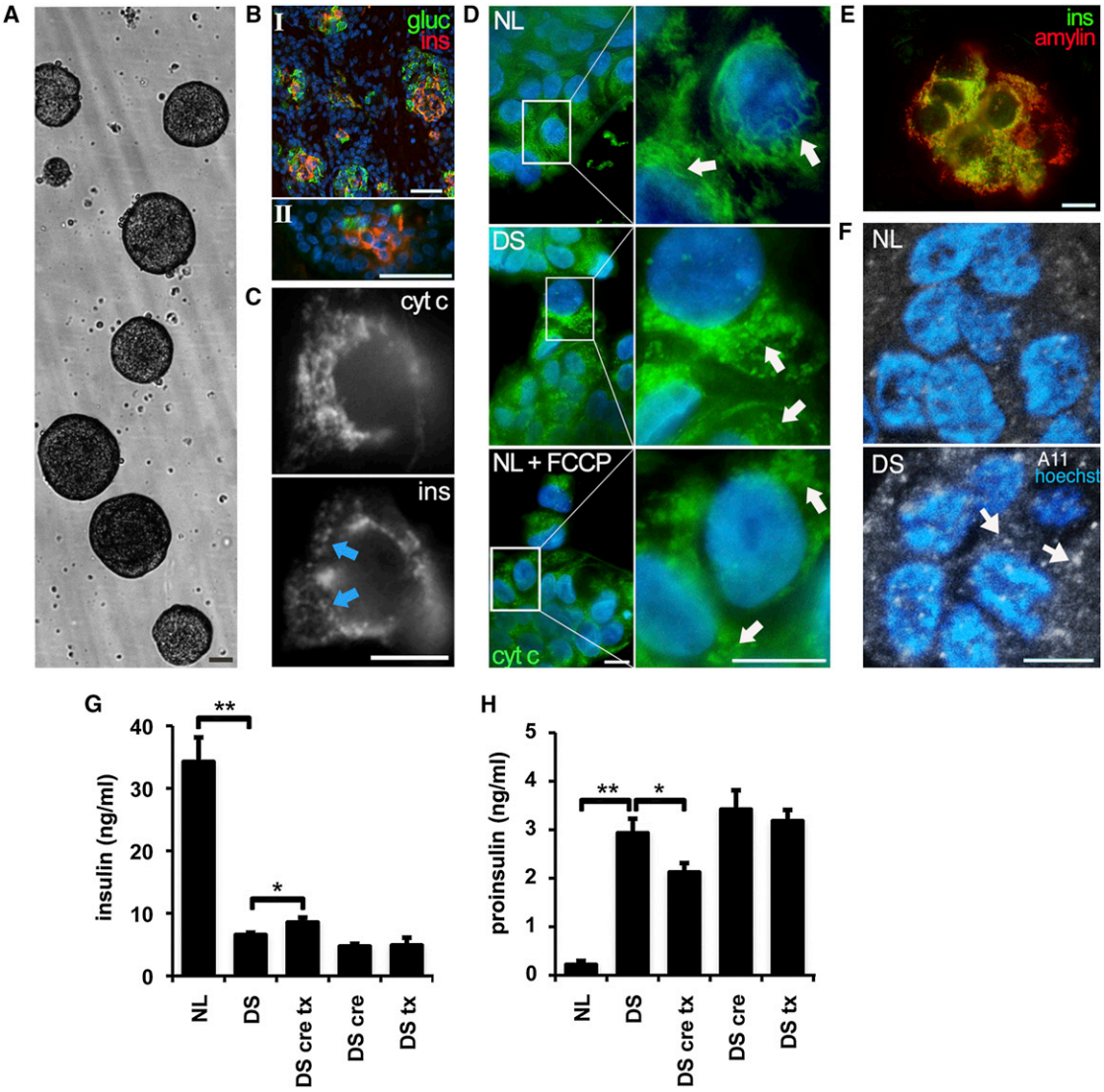


**Figure 4. Altered Mitochondrial Morphology and Function in DS Pancreatic β Cells**

(A) Fetal human pancreatic cells were grown as floating ICCs. NL and DS ICCs exhibited similar expansion rates. The scale bar represents 100 μm.

(B) β cells from the fetal pancreas (subpanel I) and ICCs (subpanel II) express insulin (ins, red) and glucagon (gluc, green). The scale bar represents 100 μm.

(C) Mitochondria visualized in an insulin-positive cell (ins, arrows) with anti-cytochorome C IF (cyt c). The scale bar represents 10 μm.

(D) Mitochondria were stained in β cells as described in (C). Note the increase in fragmented mitochondria in DS ICCs and in NL ICCs exposed to the electron transport chain uncoupler FCCP (NL+ FCCP). The scale bar represents 10 μm.

(E) Colocalization of insulin and IAPP (amylin) in ICC β cells. The scale bar represents 10 μm.

(F) A11 imunoreactivity in DS ICCs. Sections of NL and DS ICCs were labeled with antibody A11, which recognizes IAPP oligomers. Note the increase in A11 staining in DS β cells (arrows). Nuclei were stained with DAPI. The scale bar represents 10 μm.

(G) Reduced basal insulin secretion in DS ICCs. Insulin secretion was measured in ICC conditioned medium. Note the small but significant increase in insulin secretion in DS ICCs treated with 50 μM trolox and 5 mM creatine (DS cre tx). $^{*}p < 0.05$ and $^{**}p < 0.01$.

(H) Higher proinsulin secretion in DS ICCs. Note the marked increase in proinsulin levels in conditioned media of DS ICCs. Combined treatment with trolox and creatine reduced proinsulin secretion in DS ICCs. $^{*}p < 0.05$ and $^{**}p < 0.01$.

(G and H) Statistics: one-way ANOVA followed by Tukey's HSD test. Values are the mean ± SD; n = 5 independent experiments.

samples (Busciglio et al., 2002). The protocol for tissue procurement complied with federal and institutional guidelines for fetal research. Each experiment was replicated with at least five different normal and DS cultures. For most experiments, cortical neuronal and astrocyte cultures were used at 30–35 days in vitro. Fetal pancreatic cultures were generated from NL and DS fetal pancreases as described (Beattie et al., 1997). Mitochondrial and endocrine precursor cell function was analyzed at day 5 in culture.

### Imaging

Fluorescent images were generated with a Zeiss Axiovert 200 inverted microscope, and image analysis was performed with AxioVision software customized macros. Mitochondria were classified by length intervals or according to predetermined sizes as punctate, tubular, and globular and scored using AxioVision. Mitochondrial transport and quantification of mobile mitochondria were measured by time-lapse image analysis after a 20 min incubation with

100 nM MitoTracker Green (detailed in Supplemental Experimental Procedures).

### Assessment of Mitochondrial Function

Mitochondrial ox/red was measured using the MTS assay (Promega, Madison, WI, USA). JC-1 (Invitrogen) was used for assessing MMP as a ratio between the JC-1 red area (high-MMP mitochondria) and the JC-1 green area (total mitochondria) after incubation with 200 nM JC-1 for 20 min. A lactate dehydrogenase (LDH) assay was used for assessing cell density (CytoTox 96, Promega). ATP levels were measured using chemiluminescence (CellTiter-Glo, Promega). For all experiments, lipid peroxidation, ox/red, and ATP levels were normalized to LDH cellular levels or total protein content. Both normalization methods gave similar results.

### Transfection

Cells were transfected with Lipofectamine (Invitrogen), and the plasmid of interest was transfected in a ratio of 0.4 μg of DNA plus 1 μl of Lipofectamine per 500 μl of medium. Full-length mitofusin 1 and mitofusin 2 plasmids (pmfn1 and pmfn2; Origene, Rockville, MD, USA) and mitochondrial-targeted cyan fluorescent protein (pCFPmit) vector (Clontech, Palo Alto, CA, USA) were confirmed via sequencing. Plasmid concentrations were selected after dose-response curves were performed for finding the optimal conditions for stimulating fusion but avoiding hyperfusion of the mitochondrial network. At the indicated concentrations, none of the vectors caused hyperfusion, nor did they affect cell viability.

### Immunocytochemistry

Cell cultures and ICCs were fixed with 4% paraformaldehyde-0.12 M sucrose in PBS and permeabilized with 0.1% Triton X-100 in PBS. Immunofluorescent preparations were visualized using Alexa-conjugated secondary antibodies (Invitrogen), as previously described (Helguera et al., 2005; Beattie et al., 1997). The following primary antibodies were used: sheep anti-cytochrome C (Abcam, Cambridge), rabbit anti-insulin (clone C27C9, Cell Signaling, Danvers, MA, USA), mouse anti-IAP (Serotec, Raleigh, NC, USA), conformation-specific anti-oligomeric amyloid (A11, kindly provided by Dr. C. Glabe, University of California, Irvine).

### Gene Expression

Profiles were generated using total mRNA from NL astrocytes, NL astrocytes treated with $H_2O_2$ (50 μM for 24 hr), and DS astrocytes and hybridized onto HumanRef-8 v.2 Expression BeadChips (Illumina). See Supplemental Experimental Procedures for technical details.

### ELISA

Commercial kits for insulin (ALPCO Diagnostics, Windham, NH, USA) and proinsulin (LIMCO Research, St. Charles, MO, USA) were used according to manufacturer's instructions. Conditioned media from NL and DS floating ICCs were sampled after 5 days in culture.

### Oxidative Stress

Mitochondrial superoxide was visualized using MitoSOX Red (Invitrogen), which emits red fluorescence when oxidized by superoxide. Cells were treated with MitoSOX Red (200 nM) for 10 min and colabeled with MitoTracker Green (100 nM). The red/green ratio was used as an indicator of superoxide production per mitochondrial mass. Lipid peroxidation was detected using diphenyl-1-pyrenylphosphine (DPPP, Molecular Probes, Invitrogen). DPPP fluorescence was quantified in a SpectraMax fluorometer (Molecular Devices).

### Creatine Treatment

Cortical cultures were treated with 5 mM creatine for 7 days. ICCs were treated with 5 mM creatine for 2 days. See Supplemental Experimental Procedures.

### Statistical Procedures

Data were analyzed by one-way ANOVA followed by Tukey's honestly significant difference (HSD) test when the experiment included three or more groups and by two-way ANOVA followed by Tukey's HSD test for assays with two independent variables. Student's t test was performed for paired observations. A value of $p < 0.05$ was considered statistically significant. Results were expressed as the mean ± SD. All experiments were repeated at least three to five times, using cultures derived from different NL and DS specimens. Each individual experiment was performed in at least triplicate samples.

## ACCESSION NUMBERS

Raw microarray data sets have been deposited in the NCBI Gene Expression Omnibus (GEO) database under accession number GSE42772.

## SUPPLEMENTAL INFORMATION

Supplemental Information includes three figures and Supplemental Experimental Procedures and can be found with this article online at http://dx.doi.org/10.1016/j.cmet.2012.12.005.

## ACKNOWLEDGMENTS

We thank Drs. Alberto Hayek (UCSD), Peter Butler (UCLA), and Alfredo Lorenzo (IMMF, CONICET, and UNC) for expert advice. P.H. and G.H. are members of the National Council for Scientific and Technological Research (CONICET), Argentina. This work was supported by grants from The Larry L. Hillblom Foundation and NIH (HD38466 and Alzheimer's Disease Research Center grant AG16573).

Received: June 1, 2012
Revised: September 19, 2012
Accepted: December 10, 2012
Published: January 8, 2013

## REFERENCES

Andres, R.H., Ducray, A.D., Huber, A.W., Pérez-Bouza, A., Krebs, S.H., Schlattner, U., Seiler, R.W., Wallimann, T., and Widmer, H.R. (2005). Effects of creatine treatment on survival and differentiation of GABA-ergic neurons in cultured striatal tissue. J. Neurochem. *95*, 33–45.

Arbuzova, S., Hutchin, T., and Cuckle, H. (2002). Mitochondrial dysfunction and Down's syndrome. Bioessays *24*, 681–684.

Beattie, G.M., Cirulli, V., Lopez, A.D., and Hayek, A. (1997). Ex vivo expansion of human pancreatic endocrine cells. J. Clin. Endocrinol. Metab. *82*, 1852–1856.

Brady, S.T. (1991). Molecular motors in the nervous system. Neuron *7*, 521–533.

Brooksbank, B.W., and Balazs, R. (1984). Superoxide dismutase, glutathione peroxidase and lipoperoxidation in Down's syndrome fetal brain. Brain Res. *318*, 37–44.

Busciglio, J., and Yankner, B.A. (1995). Apoptosis and increased generation of reactive oxygen species in Down's syndrome neurons in vitro. Nature *378*, 776–779.

Busciglio, J., Pelsman, A., Wong, C., Pigino, G., Yuan, M., Mori, H., and Yankner, B.A. (2002). Altered metabolism of the amyloid beta precursor protein is associated with mitochondrial dysfunction in Down's syndrome. Neuron *33*, 677–688.

Capone, G.T., Grados, M.A., Kaufmann, W.E., Bernad-Ripoll, S., and Jewell, A. (2005). Down syndrome and comorbid autism-spectrum disorder: characterization using the aberrant behavior checklist. Am. J. Med. Genet. A. *134*, 373–380.

Chan, D.C. (2006). Mitochondria: dynamic organelles in disease, aging, and development. Cell *125*, 1241–1252.

Coskun, P.E., and Busciglio, J. (2012). Oxidative Stress and Mitochondrial Dysfunction in Down's Syndrome: Relevance to Aging and Dementia. Curr. Gerontol. Geriatr. Res. *2012*, 383170.

Esbensen, A.J. (2010). Health conditions associated with aging and end of life of adults with Down syndrome. Int. Rev. Res. Ment. Retard. *39*(C), 107–126.

Esposito, G., Imitola, J., Lu, J., De Filippis, D., Scuderi, C., Ganesh, V.S., Folkerth, R., Hecht, J., Shin, S., Iuvone, T., et al. (2008). Genomic and

functional profiling of human Down syndrome neural progenitors implicates S100B and aquaporin 4 in cell injury. Hum. Mol. Genet. *17*, 440–457.

Helguera, P., Pelsman, A., Pigino, G., Wolvetang, E., Head, E., and Busciglio, J. (2005). ets-2 promotes the activation of a mitochondrial death pathway in Down's syndrome neurons. J. Neurosci. *25*, 2295–2303.

Kayed, R., Head, E., Sarsoza, F., Saing, T., Cotman, C.W., Necula, M., Margol, L., Wu, J., Breydo, L., Thompson, J.L., et al. (2007). Fibril specific, conformation dependent antibodies recognize a generic epitope common to amyloid fibrils and fibrillar oligomers that is absent in prefibrillar oligomers. Mol. Neurodegener. *2*, 18.

Knott, A.B., Perkins, G., Schwarzenbacher, R., and Bossy-Wetzel, E. (2008). Mitochondrial fragmentation in neurodegeneration. Nat. Rev. Neurosci. *9*, 505–518.

Lott, I.T., and Head, E. (2005). Alzheimer disease and Down syndrome: factors in pathogenesis. Neurobiol. Aging *26*, 383–389.

Pallardó, F.V., Lloret, A., Lebel, M., d'Ischia, M., Cogger, V.C., Le Couteur, D.G., Gadaleta, M.N., Castello, G., and Pagano, G. (2010). Mitochondrial dysfunction in some oxidative stress-related genetic diseases: Ataxia-Telangiectasia, Down Syndrome, Fanconi Anaemia and Werner Syndrome. Biogerontology *11*, 401–419.

Park, K.S., Wiederkehr, A., Kirkpatrick, C., Mattenberger, Y., Martinou, J.C., Marchetti, P., Demaurex, N., and Wollheim, C.B. (2008). Selective actions of mitochondrial fission/fusion genes on metabolism-secretion coupling in insulin-releasing cells. J. Biol. Chem. *283*, 33347–33356.

Passos, J.F., Saretzki, G., Ahmed, S., Nelson, G., Richter, T., Peters, H., Wappler, I., Birket, M.J., Harold, G., Schaeuble, K., et al. (2007). Mitochondrial dysfunction accounts for the stochastic heterogeneity in telomere-dependent senescence. PLoS Biol. *5*, e110.

Roizen, N.J., and Patterson, D. (2003). Down's syndrome. Lancet *361*, 1281–1289.

Slonim, D.K., Koide, K., Johnson, K.L., Tantravahi, U., Cowan, J.M., Jarrah, Z., and Bianchi, D.W. (2009). Functional genomic analysis of amniotic fluid cell-free mRNA suggests that oxidative stress is significant in Down syndrome fetuses. Proc. Natl. Acad. Sci. USA *106*, 9425–9429.

Valenti, D., Manente, G.A., Moro, L., Marra, E., and Vacca, R.A. (2011). Deficit of complex I activity in human skin fibroblasts with chromosome 21 trisomy and overproduction of reactive oxygen species by mitochondria: involvement of the cAMP/PKA signalling pathway. Biochem. J. *435*, 679–688.

Williams, B.R., Prabhu, V.R., Hunter, K.E., Glazier, C.M., Whittaker, C.A., Housman, D.E., and Amon, A. (2008). Aneuploidy affects proliferation and spontaneous immortalization in mammalian cells. Science *322*, 703–709.

Yu, T., Robotham, J.L., and Yoon, Y. (2006). Increased production of reactive oxygen species in hyperglycemic conditions requires dynamic change of mitochondrial morphology. Proc. Natl. Acad. Sci. USA *103*, 2653–2658.

**Cell Metabolism, Volume *17***

# Supplemental Information

## Adaptive Downregulation of Mitochondrial Function in Down Syndrome

Pablo Helguera, Jaqueline Seiglie, Jose Rodriguez, Michael Hanna, Gustavo Helguera, and Jorge Busciglio

**Inventory:**

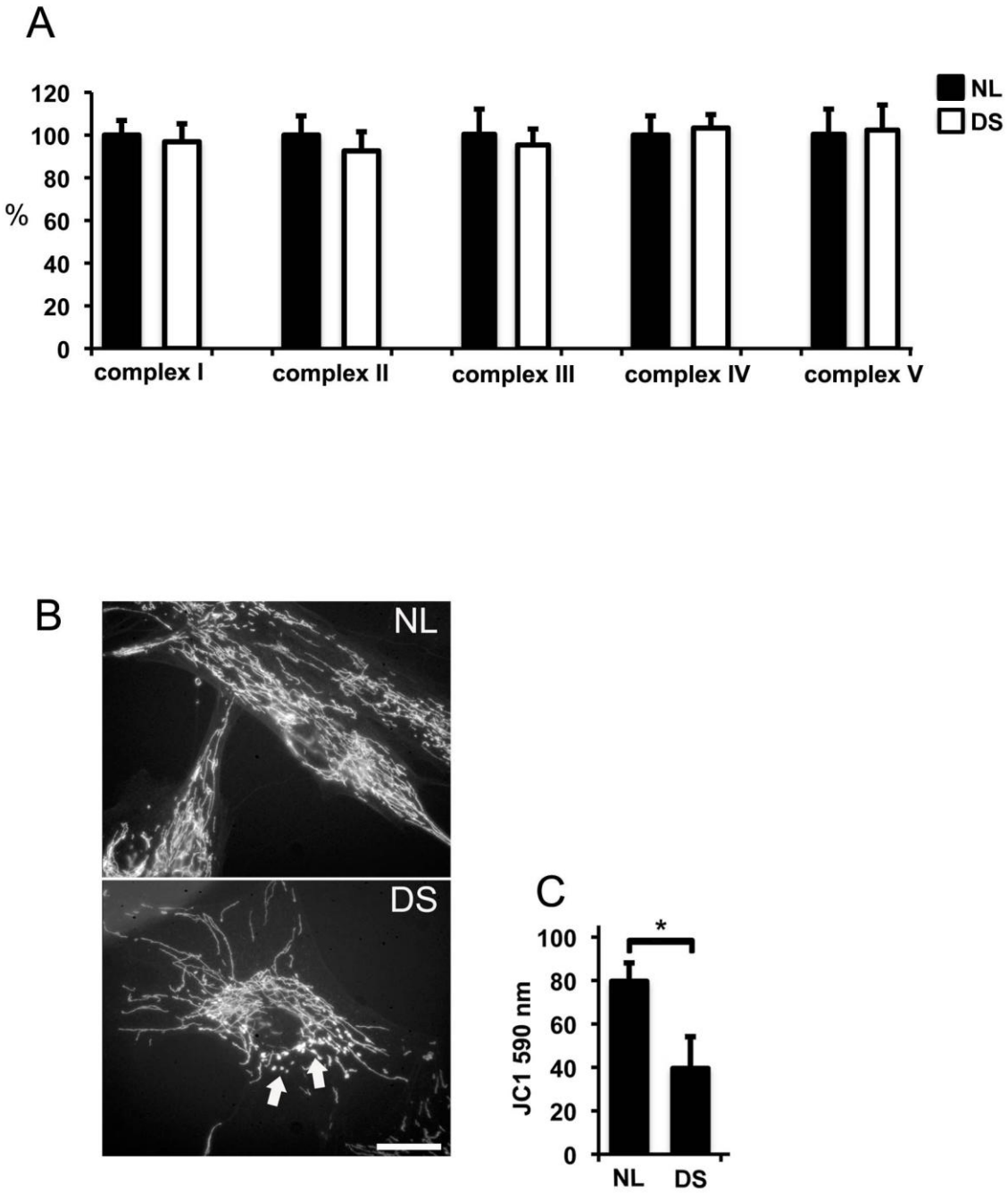


**Figure S1. Mitochondrial Protein Expression, Morphology, and Membrane Potential in DS Cells**

(A) Expression of mitochondrial complex proteins in NL and DS cells.

Proteins from the five complexes of the mitochondrial respiratory chain were quantified as described in Methods: NADH dehydrogenase, (Complex I); succinate dehydrogenase (Complex II); cytochrome C reductase, core 2 (complex III); cytochrome C oxidase, subunit IV (Complex IV); and ATP synthase alpha (Complex V). Relative protein levels were normalized as 100% in NL cultures. Similar protein levels were found in NL and DS cells. Five NL and 5 DS independent culture samples were included in the analysis.

(B) Altered morphology in mitochondria of DS fibroblasts.

Altered mitochondrial morphology in DS fibroblasts. Mitochondria in NL and DS fibroblasts were stained with Mitotracker green. There is a higher number of shorter and globular mitochondria in DS fibroblasts (arrows, lower panel). Scale bar: 10 µm.

(C) Reduced mitochondrial membrane potential in DS fibroblasts.

There is a significant decrease in JC-1 red emission (590 nm) in DS fibroblasts, Three NL and three DS cell lines obtained from ATCC were included in the analysis. Donor ages: NL 26, 29 and 29 years; DS 27, 27 and 34 years. *$p<0.05$ by Student's *t* test.

A

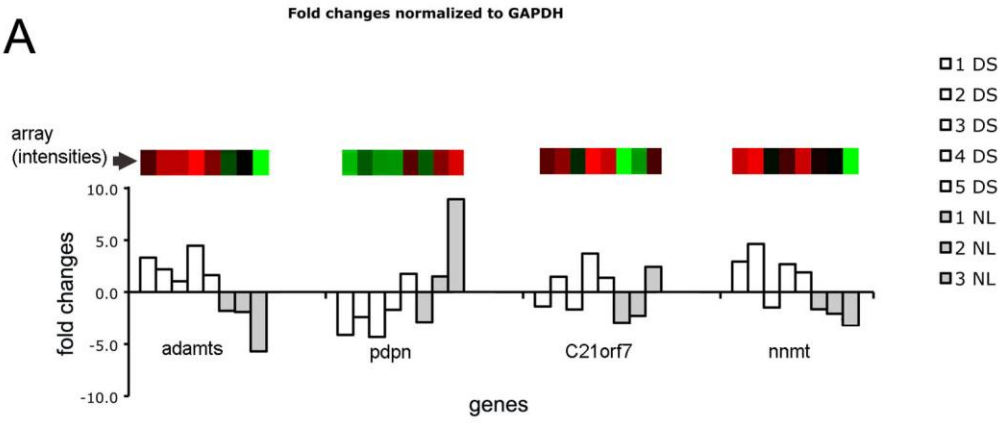
Fold changes normalized to GAPDH
array
(intensities)
1 DS
2 DS
3 DS
4 DS
5 DS
1 NL
2 NL
3 NL
10.0
5.0
0.0
-5.0
-10.0
fold changes
adamts
pdpn
C21orf7
nnmt
genes

B

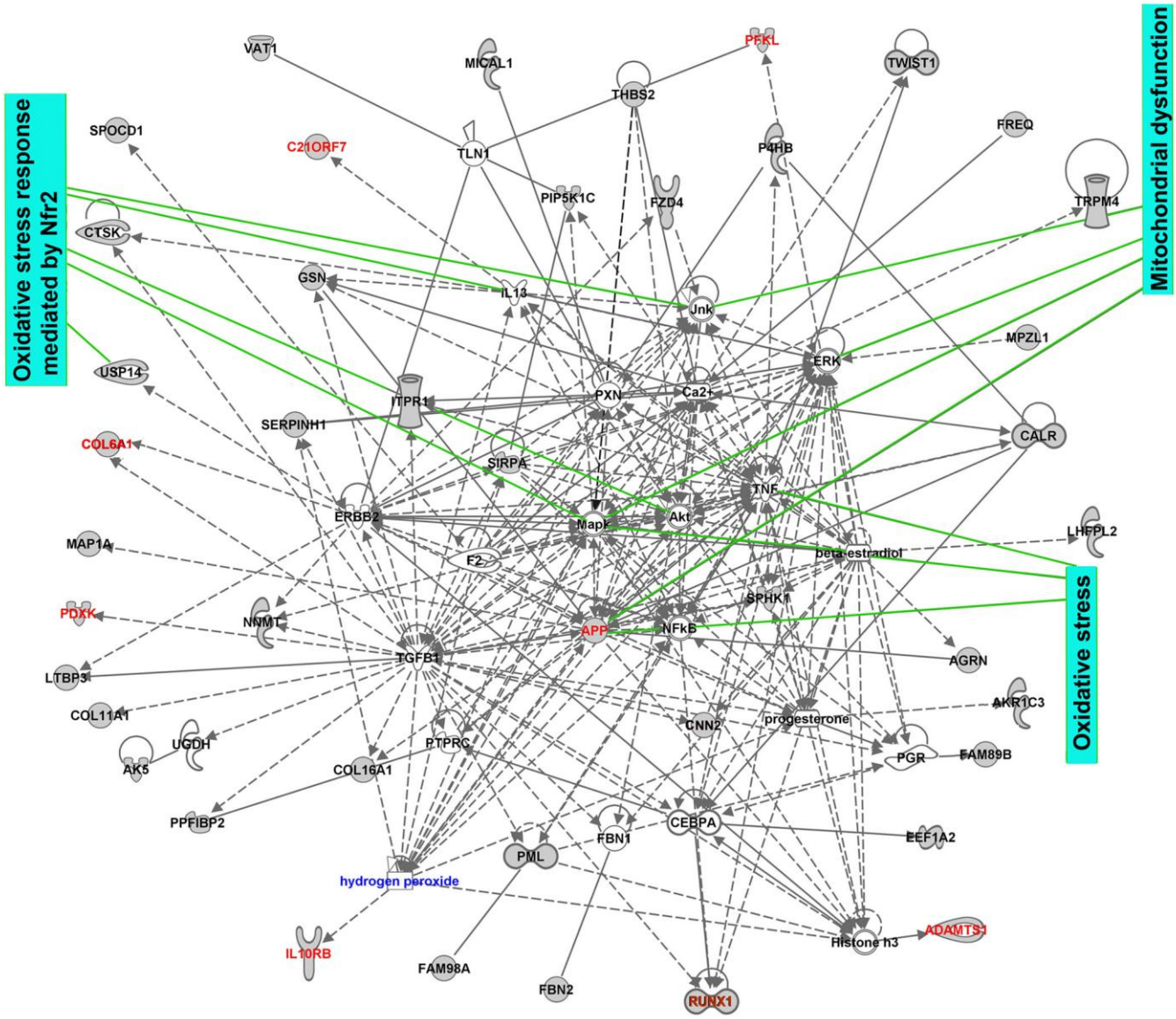
Oxidative stress response mediated by Nfr2
Mitochondrial dysfunction
Oxidative stress
VAT1
MICAL1
PFKL
TWIST1
THBS2
SPOCD1
C21ORF7
TLN1
P4HB
FREQ
PIP5K1C
FZD4
TRPM4
CTSK
GSN
IL13
Jnk
MPZL1
ERK
USP14
ITPR1
PXN
Ca2+
SERPINH1
CALR
COL6A1
SIRPA
TNF
ERBB2
Mapk
Akt
LHFPL2
MAP1A
F2
beta-estradiol
SPHK1
PDXK
NNMT
APP
NFkB
TGFB1
AGRN
LTBP3
AKR1C3
COL11A1
CNN2
progesterone
UGDH
PTPRC
PGR
FAM89B
AK5
COL16A1
PPFIBP2
CEBPA
EEF1A2
FBN1
PML
hydrogen peroxide
ADAMTS1
Histone h3
IL10RB
FAM98A
FBN2
RUNX1

**Figure S2. PCR Validation of Microarray Results and Network of Upregulated Genes in DS Cells**

(A) Quantitative PCR validation of microarray results.

Comparative results from the microarray profile presented in Fig 4 and quantitative PCR using aliquots from the same RNA purifications for four different genes (*adamts*, *pdpn*, *C21orf7*, and *nnmt*). Fold changes were normalized against GAPDH. Customized probe sets TaqMan® for the tested genes (*adamts1*, *pdpn*, *C21orf7* and *nnmt*) rendered similar results than the array output.

(B) Network of functionally related, DS upregulated genes..

A network of functional interactions was generated by Ingenuity analysis. The cluster incorporates the main networks in which DS overexpressed genes are involved (shapes in grey). Genes located in chr 21 are highlighted in red. Three pathways were identified as related to upregulated genes, 1- Nfr2-associated oxidative stress response genes, 2- oxidative stress, and 3- mitochondrial dysfunction. All three pathways support the presence of chronic oxidative stress in DS cells.

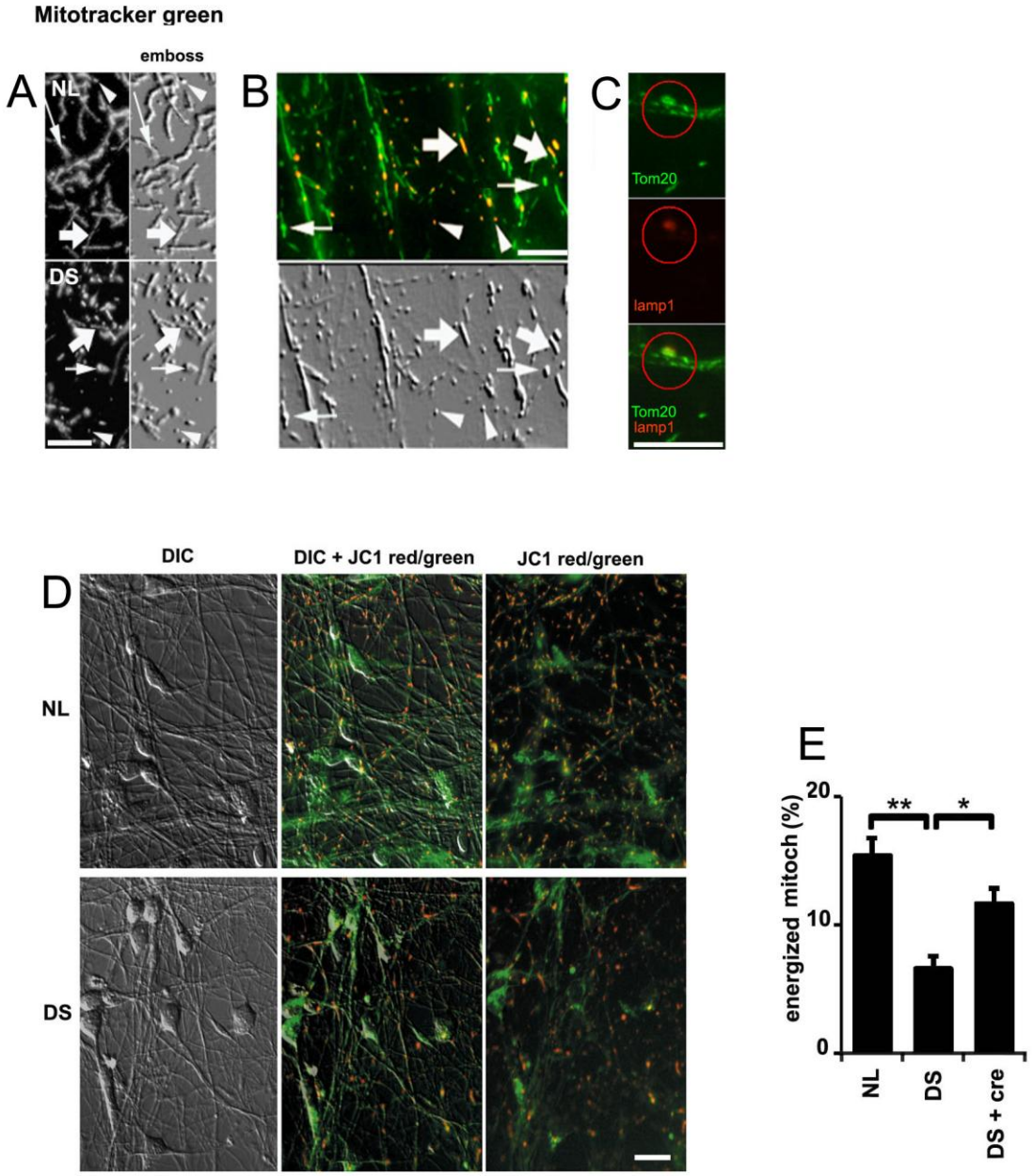


**Figure S3. Figure S3. Abnormal Mitochondrial Morphology and Membrane Potential in DS Neurons**

Mitochondrial Morphology Is Altered in DS Neurons. Visualization of mitochondria on live NL and DS cortical cultures. (A) Mitotracker green staining. Different mitochondrial morphotypes can be observed (right panels, emboss filter): tubular (arrow), globular (small arrow) and puncta-like mitochondria (arrowhead). Scale bar: 5 µm.

(B) JC-1 staining. Mitochondria were labeled with 200 nM JC-1 as described in the Supplemental Methods section. The upper panel shows the merged image of green and red fluorescent channels. The lower panel shows the same image processed with the emboss filter to enhance visualization of mitochondrial morphologies: tubular (arrow),

globular (small arrow) and puncta (arrowhead). Red fluorescence illustrates regions of higher MMP. JC-1-red staining is observed in tubular and puncta-like but not globular mitochondria. Scale bar: 5 µm.

(C) Globular mitochondria colocalize with lysosomal markers. Double IF using anti-Tom20 (green) to label mitochondria and anti-Lamp1 (red) to label lysosomes. Globular shaped mitochondria (highlighted by red circles) frequently colocalize with lamp1 IF, suggesting ongoing mitophagy of dysfunctional or damaged mitochondria. Scale bar: 5 µm.

(D) General view of energized mitochondria in NL and DS neurons. Cultures were stained with JC-1. Left panels, differential interference contrast (DIC) images. JC-1 aggregation was evident in neuronal processes in both NL and DS cultures (center and right panels). Note that energized mitochondrial regions are more abundant in NL than in DS cells. Scale bar: 10µm.

(E) Creatine increases the number of energized mitochondria in DS neurons. The histogram shows the percent of energized mitochondria (JC-1 red) with respect to total mitochondria (JC-1 green). Note the marked reduction in energized mitochondria in DS neurons and the significant increase after treatment with 5 mM creatine. *$p<0.05$ and **$p<0.01$ by one way ANOVA followed by Tukey HSD test.

## SUPPLEMENTAL EXPERIMENTAL PROCEDURES

Brain cell cultures

This study is part of an ongoing research protocol approved by the Health and Hospital Corporation of the City of New York, the Albert Einstein College of Medicine Committee on Clinical Investigation and the Internal Review Board of the University of California-Irvine. The protocols for obtaining post-mortem fetal brain tissue comply with all federal and institutional guidelines with special respect for the confidentiality of the donor's identity. Written informed consent was obtained from all tissue donors.

Primary human neuronal and astrocyte cultures were established from 10 DS brain samples (17-20 weeks of gestational age) and 10 age-matched controls, as previously described (Busciglio and Yankner, 1995). Neuronal cultures were obtained by plating dissociated human fetal cortical cells in polylysine-treated plates or coverslips. To avoid widespread DS neuronal degeneration in culture (Busciglio and Yankner, 1995) we prepared high density cultures (600 cells/mm$^2$) which were maintained in Neurobasal medium plus N2 supplement (Invitrogen, Carlsbad, CA, USA). Under these conditions, DS cortical neurons survived well, developed an extensive network of processes, and appeared no different than NL cultures in terms of morphological features. Astrocyte cultures were obtained by plating cortical cells without polylysine and removal of non adherent cells 12 hr after plating. Astrocytes were maintained in DMEM supplemented with 10% calf bovine serum (Invitrogen). Immunocytochemical staining showed that neuronal cultures were >95% positive for neuronal microtubule-associated protein 2 (MAP II) and astrocyte cultures were positive for glial fibrillary acidic protein (GFAP). Each experiment was replicated with at least 5 different normal and DS cultures. For most experiments, cell cultures were fixed or harvested at 30-35 days in vitro.

Fetal pancreatic cultures

Fetal pancreatic cultures were generated from NL and DS fetal pancreases as previously described (Beattie et al., 1997; Beattie et al., 1994). Free-floating islet-like cell clusters (ICCs) 50-150 µm in diameter were maintained in RPMI-1640 supplemented with 10% human serum and antibiotics. Hepatocyte growth factor (HGF, 25 ng/ml, SIGMA, St Louis, MO, USA) was added to stimulate and maintain the secretory phenotype in precursor cells (Hayek et al., 1995). Mitochondrial morphology and function as well as endocrine precursor cell function in ICC were analyzed after 5 days in culture. By this time, cultures have undergone significant growth, and endocrine precursor cells secrete measurable basal levels of insulin (Demeterco et al., 2000).

Transfection

The efficiency of transfection was approximately 5% for neurons and 15% for astrocytes, and the efficiency of cotransfection has been previously established in human neuronal cultures to be close to 95% (Helguera et al., 2005).

Dotblot

Cell lysates (30 µg total protein per well, 5 repetitions of each sample) were applied to an Immobilon-P membrane (Millipore, Billerica, MA, USA), probed with antibodies against mitochondrial complexes, and visualized with a green fluorescent-conjugated secondary antibody (488 nm Alexa-conjugated secondary antibody; Invitrogen). Blots were visualized and quantified using a Typhoon laser scanner (GE Healthcare Bio-Sciences, Piscataway, NJ).

Mitochondrial network analysis

Mitochondria were imaged by three different techniques. An esmboss digital filter was applied in Photoshop to facilitate mitocohondrial visualization. Cytochrome C immunostaining: Cultures were fixed, immunostained with anti cytochrome C antibody (1:1000) and visualized with an Alexa Fluor 488-conjugated secondary antibody.

Mitotracker green dye: Living cells were incubated with 100 nM Mitotracker green (Invitrogen) for 10 min, rinsed and visualized with an inverted fluorescent microscope. Mitotracker green is incorporated into mitochondrial membranes independently of the mitochondrial membrane potential.

JC-1 dye: Alternatively, mitochondrial images were generated from live cells incubated for 10 min with 200 nM JC-1 (Molecular Probes) in Hank's medium, rinsed and visualized in the green channel.

For image analysis, 20 microscopic fields per culture were acquired at 630X final magnification for neurons and ß-cells, and 200X for astrocytes, at a resolution of 1024X1024 pixels, and corrected for small inconsistencies in illumination. Stained objects were classified according to pre-determined sizes, as punctate, tubular and globular morphology in neuronal cultures, or in length intervals in astrocytes and ß cells, and scored using Axiovision. Total mitochondrial density was measured using the same threshold level and measuring the area of the image occupied by mitochondria. The frequency of each mitochondrial morphology category was assessed dividing the area of each category by the total mitochondrial area. The identity of the cultures was coded to avoid bias. At least 300 objects were scored per culture. Images were obtained

using pre-determined field coordinates from at least 5 normal and 5 DS cultures for each experiment.

Oxidative stress measurements

Superoxide assay: Mitochondrial superoxide was visualized using MitoSox red (Invitrogen), a mitochondrial superoxide indicator that exhibits red fluorescence when oxidized by superoxide but not by other ROS- or reactive nitrogen species. Cells were treated with MitoSox red (200 nM) in culture media for 10 min. Images were acquired 2 min after rinsing, for a total of 10 min. Costaining with Mitotracker green allowed simultaneous imaging of the entire mitochondrial network. The red/green ratio was used as an indicator of superoxide production per mitochondrial mass. Lipid peroxidation measurement: Lipid peroxidation was detected using diphenyl-1-pyrenylphosphine (DPPP, Molecular Probes- Invitrogen). When DPPP is oxidized to a phosphine oxide by peroxide it becomes fluorescent. DPPP fluorescence was quantified in a Spectramax fluorometer (Molecular Devices).

Cell density and viability assays

Lactate dehidrogenase (LDH) assays: Cell density in culture was assessed by measuring the total cellular LDH content using a commercial kit CytoTox 96® (Promega, Madison, WI, USA). Briefly, after cell lysis, LDH was measured with a coupled enzymatic assay, which results in conversion of a tetrazolium salt into a red formazan product. The amount of color formed is directly proportional to the original number of cells in the dish. For all experiments, lipid peroxidation (DPPP assay), oxido reductase activity and ATP levels were normalized to LDH cellular levels or total protein content. Both normalization methods gave similar results.

Propidium iodide assay: Cell viability during live imaging experiments was monitored using PI as previously described (Busciglio and Yankner, 1995).

Mitochondrial transport.

Living NL and DS neuronal cultures were stained with Mitotracker green and imaged with a 63X objective, every 2 sec in a 30 sec period. Transport velocity (nm/sec) was determined by tracking of individual objects moving anterogradely through the axon in at least 20 cells per condition in triplicate experiments.

Quantification of mobile mitochondria.

Ten second-gapped time lapse mitochondrial images (Mito Tracker Green) were subtracted after binary conversion using Image J. Overlapped mitochondria from

overlaying first and last frames were subtracted from the original last frame (subtracted 2nd image). The ratio between the subtracted 2nd image and original 2nd image represents mobile mitochondria. Ten fields from 5 different cultures were used for each experimental condition.

Assessment of energized mitochondria.

Pixel density in mitochondrial images obtained with JC-1 in both green and red channels representing total mitochondrial area (green channel) and energized mitochondrial area (red channel) were utilized to generate a JC-1 red/JC-1 green ratio. The analysis was performed in 10 fields from 5 different cultures per experimental condition.

Creatine treatment

Creatine is an organic acid that serves as endogenous substrate for creatine kinases and thereby supports cellular ATP levels exhibiting neuroprotective effects (Li et al., 2004; Andres et al., 2005). Cortical cultures were treated with 5 mM creatine for 7 days, while islet cell cultures were treated with 5 mM creatine for 2 days.

Microarray hybridization, data analysis and quantitative PCR validation

Astrocyte cultures were used for this analysis. Samples of total mRNA from normal control cultures (NL), normal cultures treated with $H_2O_2$ (50 µM for 24 hr) and DS cultures were quantified, their integrity evaluated using a Bioanalyzer system (Applied Biosciences), and hybridized onto HumanRef-8 v2 Expression BeadChips (Illumina, Inc.) at the UCLA DNA microarray facility. Global gene expression profiles for these samples, based on probe level identification of approximately 24,500 RefSeq transcripts, were collected using the BeadArray software package and analyzed using 20,589 identified probes.

Data processing was carried out using the R language for statistical computing (http://www.r-project.org); specifically, we employed the Lumi package (Lin et al., 2008) supplied by the Bioconductor Project (http://www.bioconductor.org). Prior to any differential expression analysis, raw expression values were normalized using a variance stabilizing transform. Then a probe-level quantile normalization of probes within each array and between arrays was performed separately for each biological condition to account for potential variations in mRNA background distributions. Individual conditions were finally normalized to the average of all conditions, so that relative changes in expression for a given sample represent fold changes greater than or less than the overall average. Present or absent flags were determined by the Bead Array software; probes that met a threshold of confidence (Th = 0.99) obtained based

on intensity readings of the 20,589 Illumina probes with respect to non-specific probes. A list of total genes found present in NL and DS was used for all subsequent analyses. Normalized expression profiles were used to compare between NL and DS cells. Comparison statistics were generated by a linear model approach for the analysis of data supplied by the Limma package (Wettenhall and Smyth, 2004) using an empirical Bayes method. For replicate probes within arrays a pooled correlation method was used. Differences in gene expression were considered statistically significant based on a regularized Bayesian test. Differential gene expression was measured in terms of log-ratios and filtered by statistical significance. To estimate the *p*-value a regularization of the standard Student's *t* test was implemented as described (Baldi and Long, 2001; Long et al., 2001). Signal-to-detection function was fairly constant across the entire dataset. Fold changes of NL versus DS cells samples were used to identify genes that were found to be significantly up or down regulated ($p<0.05$). Filtered genes were used for downstream analysis. After quality control, pre-processing, and data normalization of whole genome expression profiles, genes were clustered based on expression changes using the Euclidean Distance algorithm displaying Centroid Linkage (Gene Cluster program version 3.0), and visualized using the Java Tree View software. Differentially upregulated genes in DS cells were analyzed using Ingenuity Pathways Knowledge Base (http://www.ingenuity.com), a literature-based hand-curated database that allowed us to further analyze our results using well-established protein interaction pathways and to filter out false positives. We queried this database via a web-based entry tool using Illumina IDs. For qPCR validation, samples of 5 μg of each mRNA used for the microarray studies were reverse transcribed using the High Capacity cDNA Reverse Transcription kit (Applied Biosystems) according to the manufacturer instructions. Quantitative real-time PCR reactions were performed using an ABI TaqMan 7900 instrument (Applied Biosystems) with TaqMan® probe sets for GAPDH (control), PDPN, NNMT, and ADAMTS in triplicates following the manufacturer's instructions.

## SUPPLEMENTAL REFERENCES

Andres, R.H., Ducray, A.D., Huber, A.W., Perez-Bouza, A., Krebs, S.H., Schlattner, U., Seiler, R.W., Wallimann, T., and Widmer, H.R. (2005). Effects of creatine treatment on survival and differentiation of GABA-ergic neurons in cultured striatal tissue. J Neurochem 95, 33-45.

Baldi, P., and Long, A.D. (2001). A Bayesian framework for the analysis of microarray expression data: regularized t -test and statistical inferences of gene changes. Bioinformatics 17, 509-519.

Beattie, G.M., Cirulli, V., Lopez, A.D., and Hayek, A. (1997). Ex vivo expansion of human pancreatic endocrine cells. J Clin Endocrinol Metab 82, 1852-1856.

Beattie, G.M., Levine, F., Mally, M.I., Otonkoski, T., O'Brien, J.S., Salomon, D.R., and Hayek, A. (1994). Acid beta-galactosidase: a developmentally regulated marker of endocrine cell precursors in the human fetal pancreas. J Clin Endocrinol Metab 78, 1232-1240.

Busciglio, J., and Yankner, B.A. (1995). Apoptosis and increased generation of reactive oxygen species in Down syndrome neurons in vitro. Nature 378, 776-779.

Demeterco, C., Beattie, G.M., Dib, S.A., Lopez, A.D., and Hayek, A. (2000). A role for activin A and betacellulin in human fetal pancreatic cell differentiation and growth. J Clin Endocrinol Metab 85, 3892-3897.

Hayek, A., Beattie, G.M., Cirulli, V., Lopez, A.D., Ricordi, C., and Rubin, J.S. (1995). Growth factor/matrix-induced proliferation of human adult beta-cells. Diabetes 44, 1458-1460.

Helguera, P., Pelsman, A., Pigino, G., Wolvetang, E., Head, E., and Busciglio, J. (2005). ets-2 promotes the activation of a mitochondrial death pathway in Down syndrome neurons. J Neurosci 25, 2295-2303.

Li, Z., Okamoto, K., Hayashi, Y., and Sheng, M. (2004). The importance of dendritic mitochondria in the morphogenesis and plasticity of spines and synapses. Cell 119, 873-887.

Lin, S.M., Du, P., Huber, W., and Kibbe, W.A. (2008). Model-based variance-stabilizing transformation for Illumina microarray data. Nucleic Acids Res 36, e11.

Long, A.D., Mangalam, H.J., Chan, B.Y., Tolleri, L., Hatfield, G.W., and Baldi, P. (2001). Improved statistical inference from DNA microarray data using analysis of variance and a Bayesian statistical framework. Analysis of global gene expression in Escherichia coli K12. J Biol Chem 276, 19937-19944.

Pigino, G., Pelsman, A., Mori, H., and Busciglio, J. (2001). Presenilin-1 mutations reduce cytoskeletal association, deregulate neurite growth, and potentiate neuronal dystrophy and tau phosphorylation. J Neurosci 21, 834-842.

Wettenhall, J.M., and Smyth, G.K. (2004). limmaGUI: a graphical user interface for linear modeling of microarray data. Bioinformatics 20, 3705-3706.